Alexandria Journal of Science and Technology

Article

Conversion of bare corn cobs waste into sustainable and ecofriendly nanobiosorbent for effective removal of cationic basic fuchsin and methylene blue dyes from water

Mohamed E. Mahmoud [1, *], Gehan M. Nabil [2], Rana M. Tharwat [1], Amir M. Abdelfattah [1]

[1] *Faculty of Sciences, Chemistry Department, Alexandria University, Moharem Bey, Alexandria, Egypt.*

[2] *Chemistry department, College of Arts and Science, Prince Sattam bin Aabdelaziz University, Wadi Eldawasser, Riyadh, Saudi Arabia.*

**Correspondence Address:*

Mohamed E. Mahmouda: Faculty of Sciences, Chemistry Department, Alexandria University, Moharem Bey, Alexandria, Egypt, E.Mail: memahmoud10@gmail.com, Telephone number: 002-01004264031, Fax number: 00203-3911794

KEYWORDS: Bare corn cobs waste; Nanobiochar; Methylene blue and basic fuchsin dyes; Batch operational optimization; Adsorption kinetics-isotherms-thermodynamics.

Received:
June 07, 2023
Accepted:
July 16, 2023
Published:
August 17, 2023

ABSTRACT: Biochars are commonly employed as examples of sustainable biosorbents with wide and recent interests and applications in several fields including water purification from various toxic pollutants. Nanobiosorbents are mainly fabricated from agricultural, animal and industrial wastes. In the current investigation, bare corn cobs waste (BCCW) was pyrolyzed for 1 h (at 400 ^{o}C) to generate a sustainable, low-cost and ecofriendly nanobiosorbent (BCCW-NB) for further implementation as an effective material for removal of cationic basic fuchsin (BF) and methylene blue (MB) dyes from water. A nano-scaled (17 nm) was characterized for the as-prepared nanobiosorbent from the HR-TEM imaging analysis. The influence of several impacting factors (viz. pH, time, dosage, concentration, competing species and temperature) were explored and optimized for batch elimination of BF and MB dyes (5, 10 and 15 mg/L) from aqueous solution by BCCW-NB. The pH 5, 10 min and 30 mg BCCW-NB for both pollutants were characterized as the optimum condition to afford the maximum removal of both BF and MB dyes (R%>90.0%). The adsorption of BF and MB dyes followed the Freundlich isotherm and pseudo-second-order models. Finally, the potential of adsorptive elimination of BF and MB dyes from various water specimens by BCCW-NB nanobiosorbent confirmed excellent recovery with %R corresponding to 98.58%, 91.07% and 98.55% for MB and 93.45%, 90.13% and 97.89% for BF dye from drinking water, sea water and industrial waste water. Therefore, the assembled and testified BCCW-NB nanobiosorbent was confirmed as excellent low cost, sustainable and effective material for water remediation of dye pollutants.

1. INTRODCTION

Biomass waste materials have been improperly treated in a number of countries to represent a great cause for potential risks to both humans and various environments [1]. Agriculture is one of the biggest sectors with the highest fundamental and environmental inputs due to the tremendous generated agricultural wastes from corn, rice, wheat and others as engendered annually [2]. Agricultural wastes are produced annually in millions of tons from these crop residues after the collection of the grains [3]. In the past decade, corn-grain has globally increased by 40% to reach now more than 1 billion tons. In addition, stems, leaves, fastballs, husks, and bare corn cobs are the main residual components which represent about 47–50% from the corn production [4].

Online ISSN: 2974-3273

DOI: 10.21608/AJST.2023.216152.1013

Moreover, bare corn cobs are comprising large waste amounts of corn worldwide each year with approximate corn cob mass corresponding to 18-20 kg per 100 kg of corn grain production [5]. Corn cob is a rich biomass in cellulose, hemicellulose, and lignin [6] and therefore, the employment of such biomass materials in multidiscipline utilizations may be accompanied by some benefits with respect to economical view and ecological safeguard [7]. On the other hand, feedstock-based biomass from corn cob and other materials have been used to generate carbon-rich compounds with high economic benefits for soil improvement and wastewater purification [8]. Biochars represent a class of carbon-rich materials which are produced as stable byproducts from the thermochemical decomposition of multidiscipline biomasses under no or oxygen-limited atmosphere [9]. Due to their porous structures and significant surface functional groups, biochars have attracted great attention worldwide for solving the environmental problems as soil management [10], carbon sequestration [11], and water decontamination, purification and remediation from various pollutants [12] including toxic heavy metal cations and anions [13, 14], pharmaceuticals [15, 16], and dyes [17-20].

Excessive amounts of organic pollutants are daily generated from various sources as industrial effluents and other domestic activities [21]. One of the most impacting contaminants to water pollution is mainly correlated to dyes and coloring materials [22]. The number of dye materials are now exceedingly more than 100,000 types to afford over 7000 different colors. In addition, dyes may be classified as either acidic, basic, direct, reactive, vat, solubilized vat, dispersed, sulfur and solvent dyes [23]. However, 7 million tons of different dyes were annually discharged from the industrial dyeing processing into water bodies and thus generate huge amounts of wastewaters [24]. Moreover, most of the dyes are nondegradable compounds and therefore, documented as hazardous contaminants to both human and ecosystem due to their mutagenic, toxic, teratogenic and carcinogenic impacts [25, 26]. Therefore, numerous technical strategies have been adapted for dyes removal from water and wastewater systems and these include biological approaches [27], ozonation [28], advanced oxidation [29], electrochemical degradation [30], photodegradation [31], and adsorption technique [32]. Due to the simplicity, affordability, cost effectiveness, and other advantageous features, adsorption techniques have been recently recommended for removal of dyes and coloring materials using a variety of adsorbents, biosorbents and nanosorbents [32-35]. Biochars and their modified composites have recently found great interest for application in removal of dyes from aqueous matrices and wastewaters according to their associated sustainability, ecofriendly and economical characteristics [36-40].

Based on the aforementioned facts, the current study is devoted to convert and pyrolyze bare corn cobs waste at 400 ^{o}C. Moreover, the novelty in this work is focused on the design and obtaining a sustainable, low-cost and ecofriendly nanobiochar from biomass waste material by a simple preparation methodology in order to use it as an effective nanobiosorbent for removal of cationic dye pollutants as basic fuchsin and methylene blue from water in presence of various optimized experimental parameters. The as-prepared BCCW-NB nanobiosorbent has been also aimed to characterize by diverse identification techniques as FT-IR, HR-TEM, SEM, XRD, TGA and BET surface analysis to confirm the surface loaded functional groups, morphology, particle size, crystallinity, thermal stability and porosity. The successful usage of the investigated BCCW-NB nanobiosorbent in removal and purification of BF and MB pollutants from real water has been explored as the ultimate target in this work.

2. Experimental

2.1. Materials and solutions

All reagents and chemicals were of analytical grade. Methylene blue (MB) (dye content ≥82%, FW 319.85 g/mol) and basic fuchsin (BF) (dye content >85 %, FW337.86 g/mol), were purchased from Sigma-Aldrich, USA. Sodium hydroxide (>98.0%), potassium chloride (99%) and sodium chloride (99.9%) were obtained from WINLAB Chemicals. Sulfuric acid (98%), magnesium sulfate heptahydrate (99%), calcium chloride (> 99%) and ammonium chloride (> 99.8%) were purchased from VWR international Ltd, Poole, BH151 TD, England. Fresh corncobs were collected from local marked, Egypt.

2.2. Instrumentations

Various instruments were applied for characterization of corn cob biochar BCCW-NB nanobiosorbent and confirmed the successful biochar formation. BRUKER VERTEX 70 FT-IR spectrophotometer at 400-4500 cm^{-1} instrument was used for estimation the surface functional groups on the BCCW-NB nanobiosorbent. The specific surface area, pore size and pore volume of the BCCW-NB was obtained by BELSORP-mini II, BEL Japan. SEM analysis used for obtaining the pictures which illustrate the physical form of the BCCW-NB which obtained by JSM-IT200 series using the device (JEOL-JFC-1100E) for ion sputtering and Gold coating was applied for elevating the conductivity. TEM analysis was used for determining the morphology shape of the BCCW-NB by JEOL-JSM-1400Plus, Japan instrument. XRD Shimadzu lab X6100, Japan, instrument with generator utilizes 30.0 (mA) current and voltage 40.0 (kV). XRD analysis was used for determining the crystal lattice form of BCCW-NB. Temperature domain from 28.8° C to 120.5°C was applied for 5 mg of the BCCW-NB with heating rate 10°C min^{-1} and flow rate 40 mL min^{-1} using TGA-50-Schimadzu, Japan instrument . The major aim of TGA analysis is the estimation of the thermal stability of the nanobiosorbents. The Unico UV-2000 UV/Visible spectrophotometer was used for determining the absorbance values of methylene blue (MB), basic fuchsin (BF) at the maximum absorbance wavelength of the dyes 660 nm and 545 nm, respectively as listed in Table 1S (Supplementary Materials). The pH values of methylene blue (MB), and basic fuchsin (BF) dyes were measured on a calibrated pH-meter by the standard buffers (pH 4.0, 7.0 and 10.0).

2.3. Synthesis of bare corn cobs waste (BCCW-NB)

Conversion of bare corn cobs waste into the aimed nanobiochar (BCCW-NB) was performed by first removing out the seeds and husk. The collected bare corn cobs waste was cut into small pieces and dried in air and then milled to small particles to undergo pyrolysis at 400°C for 1 hour in a muffle furnace with low oxygen atmosphere. Finally, the pyrolyzed product was

mixed and washed with distilled water several times to remove all impurities. The product BCCW-NB nanobiochar was filtrated and dried in an oven at 70°C [17].

2.4. Batch adsorptive elimination studies [20, 24].

1.0 g of each dye (BF and MB) was diluted to 1 Liter solution using DDW in order to obtain 1000 mg/L stock solution from which the desired dyes concentration (5,10,15 mg/L) were obtained via dilution process. The absorbance of the dyes was determined by Unico UV-2000 UV/Visible spectrophotometer at λ_{max}= 665 and 545 nm for MB and BF, respectively. The batch elimination experiments of the two dyes by BCCW-NB was studied under the influence of variable BCCW-NB doses, contact times, initial dye concentrations, pHs, coexisting salts and temperatures. The BF and MB removals onto BCCW-NB were studied by the batch approach to get the percentage of dye uptake (%E) as stated in the following Eq. (1), while the q_e of dye at equilibrium is computed from Eq. (2) [14].

$$\%E = \frac{C_o - C_e}{C_o} X\ 100 \qquad (1)$$

$$q_e = \frac{C_o - C_e}{W/V} \qquad (2)$$

Where C_e and C_o are the final and initial concentration of dyes, V is the dye volume (L) and W (g) is the BCCW-NB nanobiosorbent mass.

The pH contribution on BF and MB elimination was performed via adjusting the pH range from 2 to 11 using NaOH and H_2SO_4. 20 mL (5, 10 and 15 mg/L) of MB or BF dyes with different pHs were mixed with 15 mg BCCW-NB nanobiochar and shaken for 10 min. The absorbance values of residual concentrations of MB and BF in the filtrates were measured on a UV-Vis instrument at λ_{max} 665 nm and 545 nm, respectively. The contribution of BCCW-NB dose on BF and MB elimination was accomplished by varying the mass from 5 to 100 mg. 20 mL (5, 10 and 15 mg/L) of MB or BF dyes with the selected BCCW-NB nanobiochar mass and shaken for 30 min and the process was completed as mentioned above. The contribution of contact time on BF and MB elimination was performed by mixing 15 mg of BCCW-NB nanobiochar with 20 mL of BF and MB dyes (5, 10 and 15 mg/L) with shaking time from 2 min and up to 20 min and the process was completed as described above. The contribution of initial dye concentrations on BF and MB elimination was established by treating 20 mL of different concentrations of BF and MB dyes (10 to 100 mg/L) with 15 mg of BCCW-NB and shaking for 30 min and the process was completed as mentioned above. The contribution of competing species on BF and MB elimination was accomplished by mixing 15 mg of BCCW-NB with 20 mL of 5, 10 and 15 mg/L of dye and 100 mg of the competing salts ($CaCl_2$, $MgSO_4$, NH_4Cl, KCl, and NaCl). All mixtures were shaken for 30 min then the process was completed as demonstrated above. The contribution of temperature on BF and MB elimination was followed by the reaction of 15 mg of BCCW-NB with BF and MB dyes (20 mL of 5, 10 and 15 mg/L) at various controlled reaction temperature (30 to 60 °C) using water thermostatic bath. These were filtrated and the absorbance values were measured as outlined above.

2.5. Potential removal of BF and MB dyes from real waters by BCCW-NB nanobiosorbent

The application of BCCW-NB for the elimination of BF and MB dyes from various actual water patterns using the batch ode. The chosen water specimens were spiked with BF and MB dyes to obtain15, 10 and 5 mg/L each and added to 15 mg of BCCW-NB. These were undergone shaking for 10 min and finally, the produced filtrates values were analyzed by a UV spectrophotometer to identify their absorbance values.

3. Results and Discussion

3.1 Characterization

Identification of the chemical and physical characteristics is important to find out the structural and surface characteristics of the as-prepared BCCW-NB nanobiosorben. Therefore, different characterization methods were applied in such investigation including FT-IR, XRD TEM, SEM, TGA and BET surface analysis.

The FT-IR spectrum of BCCW-NB nanobiosorbent as shown in **Figure 1a** is characterized by several peaks as the assigned O-H stretching vibration at 3300 cm^{-1} for hydroxyl phenolic functional group. Also, the aromaticity in BCCW-NB nanobiosorbent was confirmed by the C-H stretching vibration at 3181 cm^{-1} and aliphatic C-H symmetric stretching vibration at 2905 cm^{-1} which agree with their two bending vibration bands at 1435 and 1369 cm^{-1}. The band at 1226 cm^{-1} is assigned for stretching deformation of C-O and O-H groups. Finally, the presence of trace silicate can be confirmed by the peaks at 814 and 434 cm^{-1} for O-Si-O symmetric and bending vibrations respectively [41].

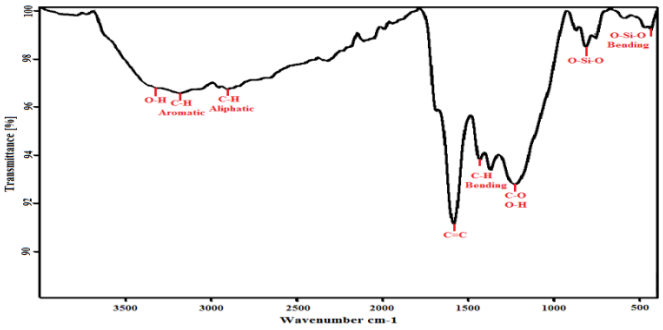

Figure 1a. FTIR of BCCW-NB nanobiosorbent

The BET surface area of BCCW-NB was identified as 9.077 m^2g^{-1} with total pore volume $2.113x10^{-2}$ cm^3g^{-1} and pore diameter 9.312 nm and the volume of gas adsorbed N_2 at STP to form an apparent monolayer on the sample surface = 2.085 cm^3g^{-1}. The adsorption-desorption isotherms was identified as a H3 type which corresponds to wedge-shaped pores formed by the stacking of flaky particles as documented by the IUPAC classification [42].

The surface morphology of BCCW-NB nanobiosorbent was evaluated from the HR-TEM and SEM images. **Figure 1b** illustrates the SEM image of this nanobiochar which refers to homogeneous individual uniform nanoparticles. Additionally, The HR-TEM image of BCCW-NB nanobiosorbent is illustrated in **Figure 1c** and show some sort of aggregation of the nanobiosorbent with an average particle size about 17 nm [43]. The XRD pattern of BCCW-NB nanobiosorbent (**Figure 1d**) shows the obvious amorphous structure of this material with a broad hump ranging from 15-30º attributed to aromatic carbon, in addition to small peak at 26.1º indicating presence of SiO_2 [44]. The thermal stability and weight loss of BCCW-NB nanobiosorbent is illustrated via TGA (**Figure 1e**) to demonstrate the loss of adsorbed moisture around 100 ºC followed by a significant mass loss at 275-528ºC due to the degradation of cellulose and hemicellulose moieties, aromatization of char and slow degradation of the remaining lignin [45].

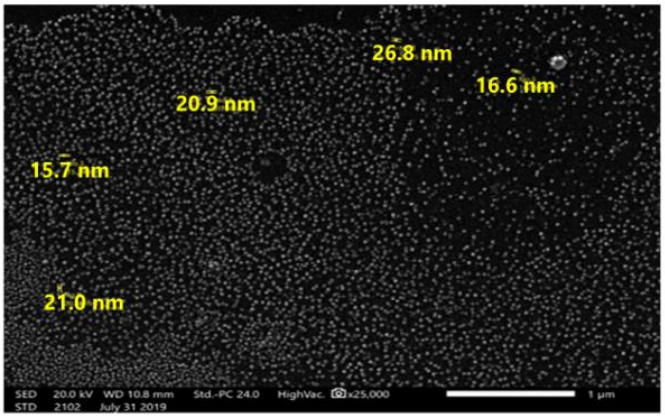

Figure 1b. SEM image of BCCW-NB nanobiosorbent

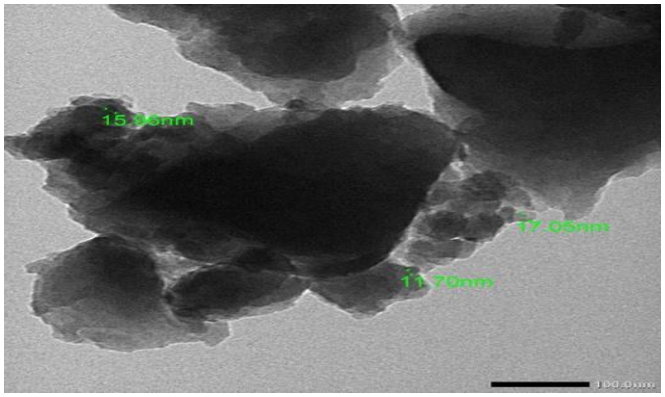

Figure 1c. HR-TEM image of BCCW-NB nanobiosorbent.

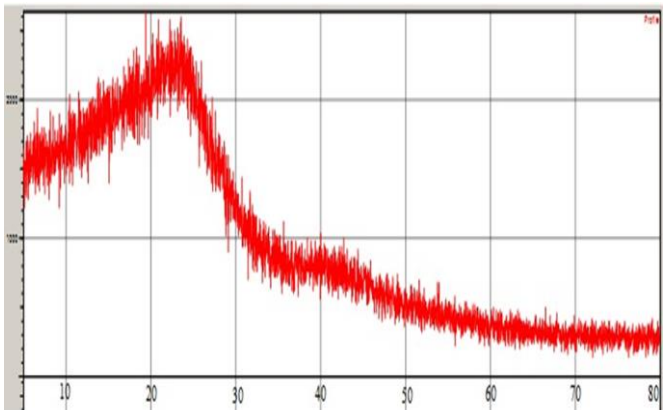

20º

Figure 1d. X-ray diffraction pattern of BCCW-NB nanobiosorbent

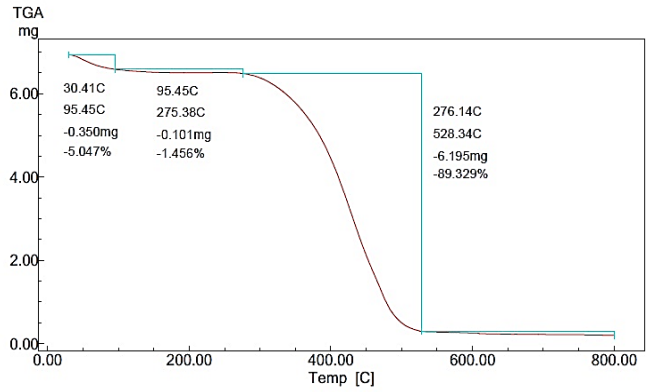

Figure 1e. TGA of BCCW-NB nanobiosorbent

3.2. Impact of several factors on the elimination of BF and MB dyes from aqueous solution by BCCW-NB nanobiosorbent

3.2.1. Contribution of pH

Since the presence of different functionalities for both the dyes as well as BCCW-NB nanobiosorbent, the interactions may be followed by attractive or repulsive forces and these are greatly affected by the medium pH. So, the impact of pH on the elimination processes of BF and MB according to their interactions with BCCW-NB is a vital factor to be examined. This was experimented by varying the pH from 1 to 11 and the collected results are compiled in Table 1. It is evident that low percent removal values were detected by both dyes at low pH and as the pH increased, these values were also increased to reach the maximum ones at pH 5. The R% of MB were corresponded to 91.71, 88.75 and 81.01% by using 15, 10 and 5 mg/L MB concentrations, respectively, While 85.22 ,82.31, 79.93% were identified for BF at concentrations 15,10 and 5 mg/L concentrations, respectively. This behavior may be due to the competition on the active surface sites between acidic protons and cationic dyes at low pH, and as the pH value

increased, the rival acidic proton concentration decreased leaving more active sites for attracting more of dye molecules [46].

Table 1. The impact of pH on percentage removal of MB and BF by BCCW-NB nanobiosorbent

Dye	Conc. mg/L	% Removal					
		pH 1	pH 3	pH 5	pH 7	pH 9	pH 11
MB	5	49.32	79.9	81.01	78.53	77.79	77.32
	10	45.92	85.43	88.76	88.69	87.21	84.31
	15	40.17	88.24	91.71	91.47	90.96	90.75
BF	5	29.07	73.26	79.33	75.23	62.28	47.13
	10	24.09	76.26	82.32	77.86	65.62	55.55
	15	18.77	78.83	85.22	81.33	75.58	71.57

3.2.2. Contribution of BCCW-NB nanobiosorbent mass dosage

In order to determine the capacity of BCCW-NB nanobiosorbent for Uptake of BF and MB, various masses were employed and varied from 5 to 100 mg. It is evident that the three investigated concentrations of MB (5, 10 and 15 mg/L) showed high efficient removal by BCCW-NB nanobiosorbent providing R% 90% by using 5 mg/L and this value was gradually increased to 95% in the case of 15 mg/L and equilibrium condition was identified at 97% upon using 30 mg dosage as illustrated in **Figure 2a**. For BF, it was found similarly behaving in the same manner with slight change as shown in **Figure 2b**. Such behaviors are mainly attributed to increasing availability of active sites on the BCCW-NB nanobiosorbent surface which favored more binding of dye molecules [47].

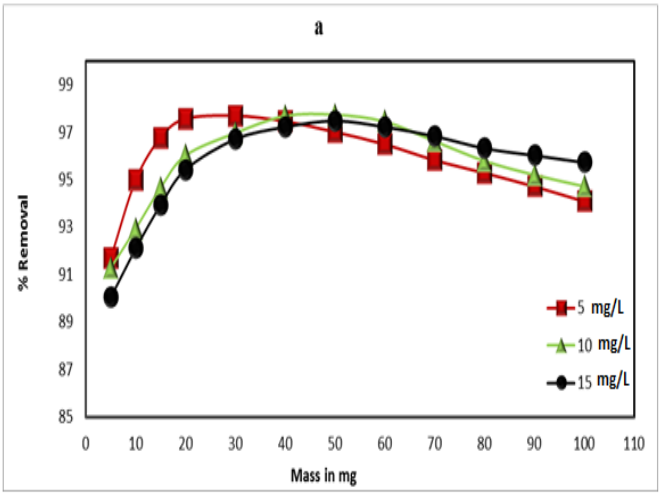

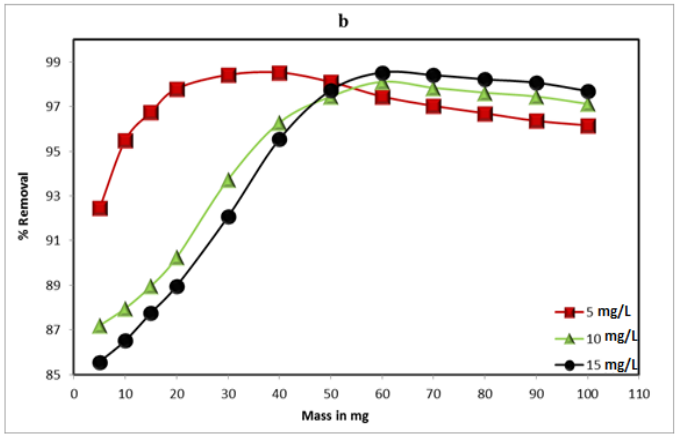

Figure 2(a, b). Effect of mass dosage on the removal efficiency of MB & BF by BCCW-NB nanobiosorbent

3.2.3. Contribution of competing salts

Three concentrations, viz. 5, 10 and 15 mg/L of both dye molecules were testified in presence of some competing salts as $CaCl_2$, $MgSO_4$, NH_4Cl, KCl, and NaCl. In case of MB, all salts were identified to compete with the uptake of MB to decrease R% for 10 and 15 mg/L concentrations, and less competition fulfilled for 5 mg/L concentration with about 70% removal as compiled in Table 2. For BF, all salts exhibited more competition in the uptake process providing a decreasing in R% for 5 and 10 mg/L concentration and less competition was accomplished in the case of 15 mg/L concentration with about 37.06% removal [48].

Table 2. Impact of competing salts on removal of MB and BF by BCCW-NB nanobiosorbent

Dye	Conc. mg/L	%Removal				
		Interfering salts				
		NaCl	KCl	NH_4Cl	$MgCl_2$	$CaCl_2$
MB	5	78.21	74.28	68.56	66.04	65.07
	10	63.41	60.55	58.05	51.89	46.28
	15	54.19	53.78	51.93	50.45	43.96
BF	5	37.06	35.63	33.75	31.11	28.35
	10	41.48	39.54	37.73	34.04	30.87
	15	37.06	35.63	33.75	31.11	28.35

3.2.4. Contribution of contact time and kinetic evaluation

The impact of contact time on the expulsion rates of BF and MB dyes by the examined BCCW-NB nanobiosorbent are represented in **Figure 3(a, b)**. The 5, 10 and 15 mg/L concentrations of BF and MB dyes were found to quickly

decrease upon interaction with BCCW-NB. The adsorption reactions were found to reach to the equilibrium at 10 min for both BF and MB dyes. At that point, the adsorption behaviors were found to decline. At the starting of this process, the adsorption rate was quick due to the increment of large number of surface-active sites and by increasing the time period the active sites turned to fully occupied by the dye molecules. So, It was gotten to be troublesome to possess empty destinations due to the shock powers between colored particles which already adsorbed on the surface which display in arrangement [49].

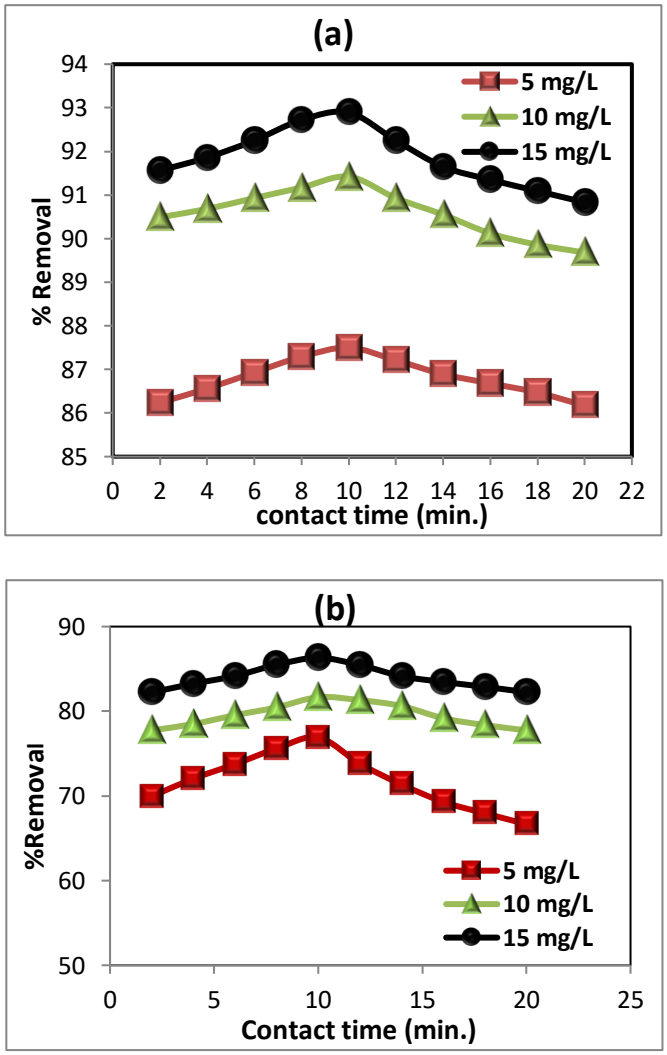

Figure 3(a, b). Effect of contact time on the removal efficiency of both MB & BF by BCCW-NB nanobiosorbent

The experimental results were also investigated by a series of kinetic parameters and models to evaluate and describe the elimination of BF and MB dyes onto BCCW-NB nanobiosorbent to characterize the most fitting model. The definitions and parameters of various linear models are stated in Table 2S (Supplementary Materials), while the computed theoretical and experimental kinetic parameters with the characterized R^2 values are stated in Table 3. Generally, the maximum R^2 reflects that such kinetic model can be employed to represent the uptake processes of BF and MB by BCCW-NB nanobiosorbent [50]. The stated *pseudo*-first order model by Lagergren [51] was mainly referring to physical adsorption nature of adsorbates as BF and MB dyes onto the adsorbent as BCCW-NB [52]. The computed R^2 values for MB and BF were in the range 0.865-0.897 and 0.785-0.884, respectively. Moreover, the $q_{e(exp)}$ was found completely different from the $q_{e(calc)}$. This confirm that the adsorption processes of both BF and MB dyes by BCCW-NB nanobiosorbent were not suitable to fit to this model.

The pseudo-second-order model was reported by Ho and Mckayis [53] and applied in this study. The collected data by this model for MB and BF dyes revealed that the $q_{e(calc)}$ were identified as 4.39, 9.16 and 13.94 mg g^{-1} as well as 3.86, 8.18 and 11.74 mg g^{-1} by using 5, 10 and 15 mg/L initial dye concentrations, respectively. These values are consistent with the experimental data, $q_{e(exp)}$ as compiled in Table 3. Moreover, **Figure 4(a, b)**. show good straight lines with R^2 values = 0.999 to prove that the adsorption of both BF and MB dyes by BCCW-NB nanobiosorbent could be suitably explained by the *pseudo*-second-order kinetic model.

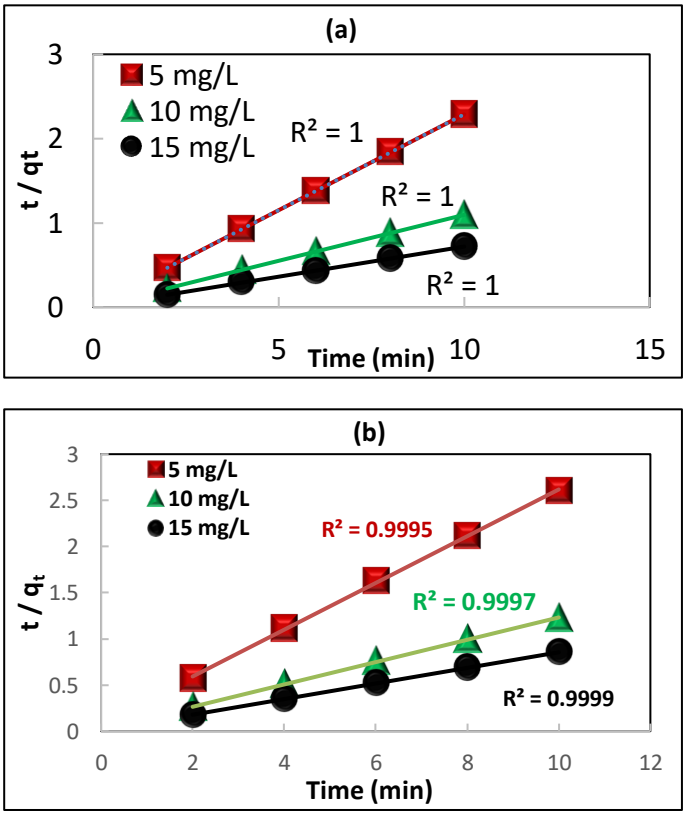

Figure 4(a, b). Pseudo-second order kinetic model for removal of MB and BF by BCCW-NB nanobiosorbent

This confirms that the suggested mechanism is mainly correlated to chemical binding between these two pollutants with BCCW-NB nanobiosorbent.

The intra-particle diffusion model proposed that the adsorption mechanism may occurred in two step, (i) transfer of solute molecules from aqueous solution to the surface of adsorbent and (ii) diffusion of adsorbate molecules into the pores of the prepared phase [54].

The collected data from plotting this models are outlined in Table 3 to refer to R^2 values 0.990, 0.973 and 0.976 for MB and 0.996, 0.965 and 0.958 for BF using the same initial concentrations of both dyes. A quick glance to Table 3, indicates that the intercept and K_{id} values was increased by increasing the initial concentration of dyes due to the liquid film mass transfer and linear portion to the intraparticle diffusion.

Table 3. Computed kinetic parameters by various models for removal of MB and BF by BCCW-NB nanobiosorbent

Kinetic model	MB dye			BF dye		
	5 mg/L	10 mg/L	15 mg L^{-1}	5 mg/L	10 mg/L	15 mg/L
Pseudo-first order q_e (mg g^{-1})(exp.) q_e (mg g^{-1})(calc.) k_1 ($min.^{-1}$) R^2	 7.480 4.390 0.209 0.974	 3.915 9.15 0.304 0.865	 1.341 13.94 0.420 0.897	 1.108 3.86 0.379 0.884	 1.404 8.18 0.382 0.785	 1.433 11.74 0.423 0.830
Pseudo-second order q_e (mg g^{-1})(exp.) q_e (mg g^{-1})(calc.) k_2 (g mg^{-1} $min.^{-1}$) R^2	 4.393 4.390 4.430 1.000	 9.165 9.150 2.903 1.000	 13.986 13.940 1.345 1.000	 3.950 3.860 0.741 0.999	 8.264 8.180 0.665 0.999	 11.834 11.74 0.721 0.999
Intraparticle diffusion K_{id}($mg.g^{-1}min^{-1/2}$) C R^2	 0.0372 4.256 0.990	 0.0536 8.966 0.973	 0.120 13.522 0.976	 0.201 3.205 0.996	 0.222 7.431 0.965	 0.211 11.045 0.958
Elovich α (mg g^{-1} min^{-1}) β (mg g^{-1}) R^2	 2.56×10^{45} 25.188 0.959	 8.54×10^{67} 17.69 0.922	 2.02×10^{45} 7.806 0.939	 11.29×10^{5} 4.651 0.971	 28.29×10^{12} 4.282 0.911	 1.28×10^{21} 4.482 0.905
Vadivelan and Vasanth Kumar model R^2	 0.973	 0.865	 0.897	 0.884	 0.785	 0.830

The Elovich model is utilized in cases of non-homogeneous systems and it is suitable for chemisorption process [55]. It is denoting to with R^2 0.959, 0.922 and 0.939 by MB and 0.971, 0.911 and 0.905 by BF dye as clarified. The better adsorption has highest value of initial adsorption rate (α) and lowest value of desorption constant (β). Finally, the evaluated Boyd kinetic model, also named Vadivelan and Vasanth Kumar model [56] was found to provide R^2 values 0.973, 0.865 and 0.897 for adsorption of MB, while 0.884, 0.785 and 0.830 for removal BF dye by BCCW-NB nanobiosorbent. Based on the Boyd model, one can conclude that the mass transfer is the rate-determining step.

3.2.5. Contribution of initial dye concentration and adsorption isotherms

The impact of initial BF and MB concentration on the adsorption process was studied using a wide concentration ranges (10-100 mg/L) at optimum conditions as represented in **Figure 5(a, b)**.

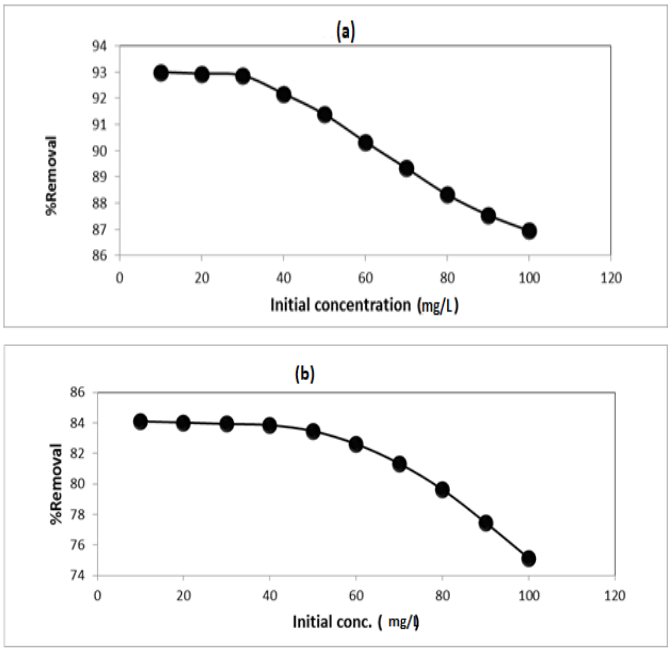

Figure 5(a, b). Effect of initial dyes concentration on removal of MB and BF by BCCW-NB nanobiosorbent

The removal efficiency (%) of BF and MB dyes was observed to decrease upon increasing the initial dye concentration. This is attributed to the increased rate of chemical binding between the interacting species. In addition, it was observed that the actual amount of removed dyes per unit mass of BCCW-NB nanobiosorbent was found to increase with the increase in the concentration of studied dyes. Such increase is mainly due to the lessen in impedance to the uptake process of dye molecules from solution. In addition, more driving force was provided in high concentration of dyes which was very necessary to overcome the mass transfer reluctance of dyes between the aqueous and solid surfaces [57]. Various adsorption isotherm models were used to relate the adsorbed amount of BF and MB by BCCW-NB with those in solution at constant temperature under equilibrium conditions. Five adsorption isotherm models were applied to investigate the isotherm data as listed out in Table 3S (Supplementary Materials). The Irving Langmuir [58] was employed to explicate the adsorption of BF and MB dyes onto BCCW-NB nanobiosorbent. It is proposed a uniform monolayer adsorption on surface without interactions between the adsorbed molecules. Straight lines were detected with R^2 values 0.989 and 0.921 for MB and BF dyes, respectively, while the characterized q_{max} values were 149.25 and 158.73 for MB and BF, respectively. All computed parameters for both BF and MB are listed in Table 4. The separation factor R_L clarifies the nature of adsorption between 0.09 – 0.499 for MB and 0.204 – 0.711 for BF dyes to indicate that the adsorption processes are favorable [59]. The Freundlich model stated that the adsorption proceed through the formation of heterogeneous surfaces with different adsorption sites. The (1/n) constant refers to Favorable, if (0 < 1/n < 1), unfavorable if (1/n > 1) or irreversible adsorption if (1/n = 0) [60]. A good line was obtained as represented in **Figure 6a** and the estimated Freundlich parameters are in Table 4. The obtained 1/n value are 0.735 and 0.804 for MB and BF, respectively, which indicate that the adsorption processes of both dyes are favorable processes but only at higher dyes concentration. The correlation coefficients (R^2) of both dyes were 0.983 and 0.972 for MB and BF dyes, separately to confirm good fitting of the adsorption data with the Freundlich model compared to the Langmuir model.

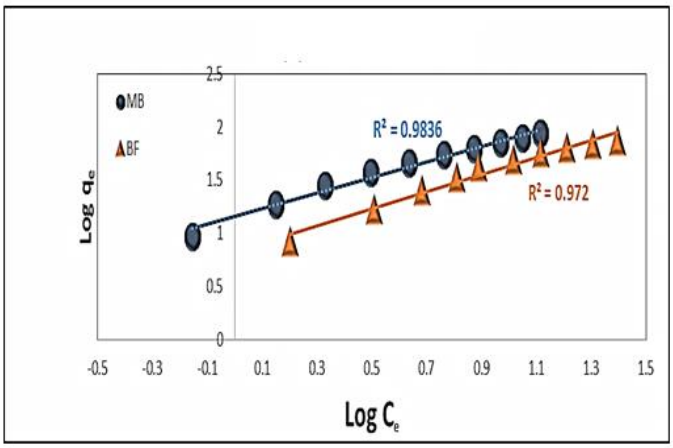

Figure 6a. Frundlice adsorption isotherm for the adsorption of MB and BF by CCBW-NB nanobiosorbent

The Temkin isotherm model predicts that the heat of adsorption is linearly declined by rising the biochar coverage [61]. The Temkin isotherm parameters are stated in Table 4 and the computed correlation coefficients R^2 by Temkin isotherm model were identified as 0.967 and 0.975 for MB and BF dyes, respectively. The Dubinin–Radushkevich (D–R) isotherm [62] doesn't predict a homogeneous surface or a constant potential of adsorption. The q_s were found 59.58 and 52.39 mg g^{-1} for MB and BF dyes, respectively, while the K_{ad} (mol^2/kJ^2) values were equal to 4×10^{-7} for MB and 1×10^{-6} for BF, with R^2 value of 0.836 and 0.804 for MB and BF, separately, as listed in Table 4. The K_{ad} values give the information about the mean free energy E (kJ/mol) of adsorption per mole of the studied dye as calculated from equation (3).

$$Es = \frac{1}{\sqrt{2\,Kad}} \qquad (3)$$

If Es >16 $kJmol^{-1}$, the adsorption process is chemisorption and if Es < 8 $kJmol^{-1}$, the adsorption process is a physisorption. The calculated Es values were equal to 1.123, 0.709 $kJmol^{-1}$ for MB and BF dyes, respectively to affirm physisorption processes [63].

Scatchard analysis plot is generally used to provide more information about the affinity of various binding sites and interpret the results of adsorption isotherms. The equation used and the parameters definitions are shown in Table 4.

Table 4. Computed parameters by various adsorption isotherm models

Isotherm model	Isotherm parameters	MB	BF
Langmuir	q_{max} (mg/g) b (L mg^{-1}) R_L R^2	149.25 0.1003 0.09 - 0.49 0.989	158.73 0.039 0.20-0.71 0.921
Freundlich	n K_f (L. mg^{-1}) R^2	1.359 14.272 0.983	1.242 6.788 0.972
Temkin	a_T (L. g^{-1}) b_T (J/mol) B R^2	1.496 92.595 26.757 0.967	0.659 94.835 26.125 0.975
Dubinin-Radushkevich	q_s (mg/g) K_{ad} (mol^2/ j^2) E_s (kJ mol^{-1}) R^2	59.584 4×10^{-7} 1.123 0.836	52.399 1×10^{-6} 0.709 0.804
Scatchard plot	High affinity	b=0.013, Q_p= 979.12, R^2 = 0.999	b=0.003, Q_p= 1604, R^2 = 0.622
	Low affinity	b=0.12, Q_p= 133.82, R^2 = 0.988	b=0.057, Q_p= 130.52, R^2 = 0.930

The shape of Scatchard plot is reflecting the type of interactions of adsorbate with the adsorbent. **Figure 6b** shows the Scatchard plot with a deviation from linearity and this means that BCCW-NB nanobiosorbent presents more than one type of binding sites, high affinity (H) and low affinity (L) due to the difference in affinities of the binding between the adjacent sites towards the adsorbed dyes. As compiled in Table 4, the calculated Q_o and b values from Langmuir are very close to those calculated from the low affinity binding sites, for the sorption of BF and MB dyes onto BCCW-NB nanobiosorbent which is attributed to low affinity binding sites.

Therefore, the binding reaction and mechanisms may involve electrostatic interactions rather than ion exchange mechanism [64].

By comparing the R^2 values for adsorption of BF and MB dyes onto BCCW-NB nanobiosorbent, one can be deduced from Table 4 that the Freundlich isotherm demonstrated most valid model for fitting the data than the other expressions.

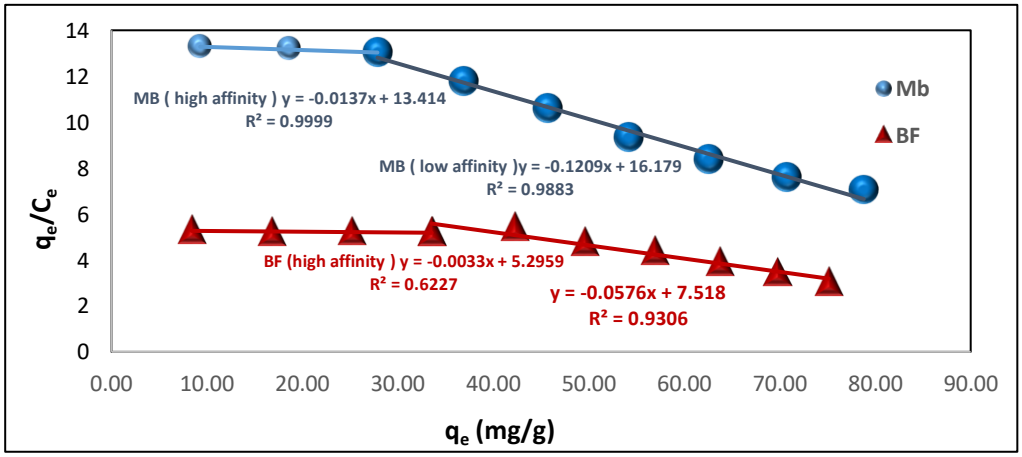

Figure 6b. Scatchard plot adsorption isotherm for the adsorption of MB and BF by BCCW-NB nanobiosorbent

3.2.6. Contribution of temperature and thermodynamic studies

The contribution of temperature is another important physico-chemical parameter because any changes in the temperature will affect the adsorption efficacy and capacity for binding of BF and MB dyes onto BCCW-NB nanobiosorbent. The impact of temperature was studied at three various dyes concentrations (5, 10 and 15 mg/L) using the selected temperatures (30, 35, 40, 45, 50, 55 and 60°C). the results are represented in **Figure 7 (a,b)**. It is explicit that a decrease in the removal efficacy (%) of BF and MB was spotted with raising the temperature. The diminution in R% at higher temperature referred to an exothermic behavior of adsorption due to the bonds among dye molecules and the active pore sites on nanobiosorbent are weak. In addition, the dissolution of dyes also raised, which caused the interaction between the solute and solvent become less than the solute and BCCW-NB nanobiosorbent. Therefore, BF and MB dye molecules were not easy to be adsorbed [65].

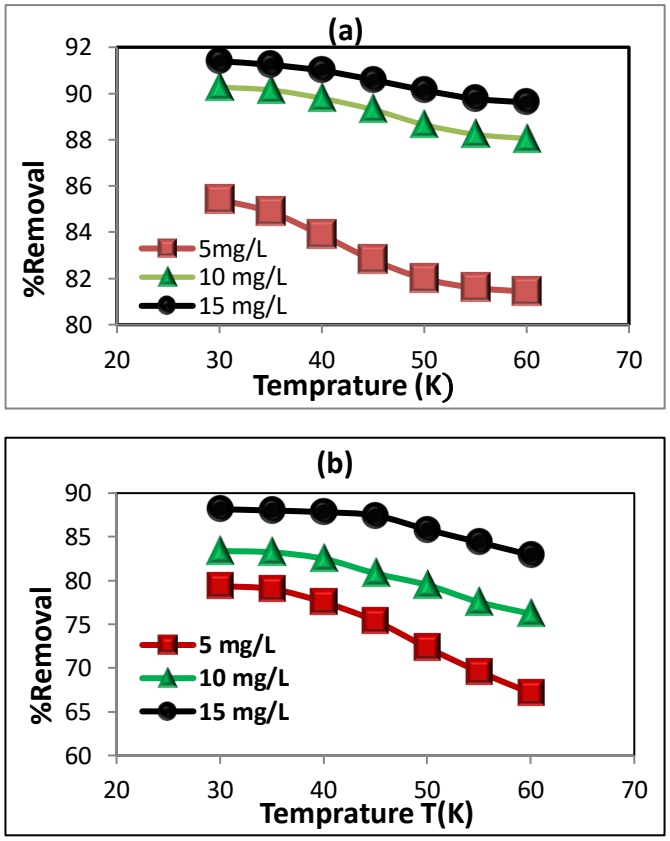

Figure 7 (a,b). Effect of temperatures on the adsorption of MB and BF by BCCW-NB nanobiosorbent

The standard thermodynamic parameters: standard Gibbs free energy (ΔG°), standard enthalpy change (ΔH°) and standard entropy change (ΔS°) at different temperatures are enclosed in Table 5. ΔG° is given by Eq. (4).

$$\Delta G^\circ = -RT \ln K_d \qquad (4)$$

K_d (L/g) is the equilibrium sorption constant given by Eq. (5).

$$K_d = q_e V / C_e W \qquad (5)$$

q_e (mg/g) and C_e (mg/L) as mentioned before, V is for dye solution (L) and W is the mass of biochar (g). (ΔH°) and (ΔS°) of BF and MB are presented by Van't Hoff according to Eq. (6).

$$\ln K_d = \frac{\Delta S^o}{R} - \frac{\Delta H^o}{RT} \qquad (6)$$

The ΔS° and ΔH° are obtained from the slope and intercept as given in **Figure 8 (a,b).** The outlined results in Table 5 show negative ΔG° values to confirm the spontaneity of the adsorption process, but the elimination of dyes become more favorable at lower temperatures. The negative values of ΔH° emphasized that BF and MB adsorption reaction were exothermic in nature [66] The negative ΔS° values, suggest more ordered molecules at the liquid-solid interface during BF and MB adsorption. But the negativity is decreasing by increasing the initial dyes concentration indicating the increase in randomness at solid-liquid interface [67].

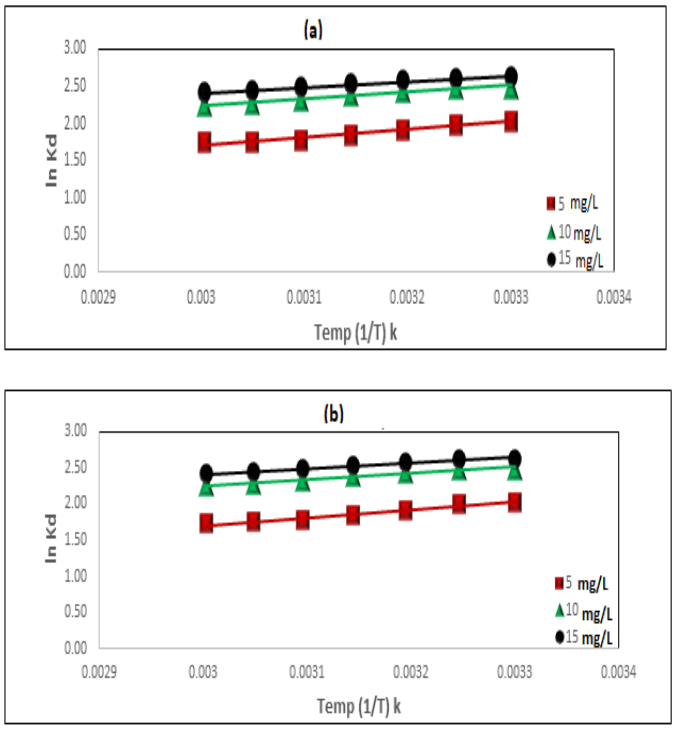

Figure 8 (a,b). Vant Hoff s plot for the adsorption of adsorption of MB and BF by BCCW-NB nanobiosorbent

Table 5. The collected standard thermodynamic parameters for adsorption of MB and BF by BCCW-NB nanobiosorbent at different temperatures

Initial dye (mg/L)	Adsorption Thermodynamic Parameters															
	MB dye														ΔS° (J/mol.K)	ΔH° (KJ/mol)
	Kd (L/g)							- ΔG° (KJ/mol)								
	303K	308K	313K	318K	323K	328K	333K	303K	308K	313K	318K	323K	328K	333K		
5	7.61	7.29	6.77	6.26	5.92	5.76	5.70	5.11	5.09	4.98	4.85	4.77	4.78	4.82	-12.442	-8.870
10	12.06	11.90	11.43	10.86	10.15	9.74	9.58	6.27	6.34	6.34	6.31	6.22	6.21	6.26	-3.036	-7.243
15	13.82	13.54	13.14	12.51	11.88	11.41	11.21	6.62	6.67	6.70	6.68	6.65	6.64	6.69	+0.813	-6.404
BF Dye																
Kd (L/g)								- ΔG° (KJ/mol)							ΔS° (J/mol.K)	ΔH° (KJ/mol)
5	5.00	4.90	4.48	3.98	3.40	2.97	2.66	4.06	4.07	3.90	3.65	3.29	2.97	2.71	-12.442	-8.870
10	6.52	6.44	6.12	5.48	5.04	4.49	4.16	4.72	4.77	4.72	4.50	4.34	4.09	3.95	-3.036	-7.243
15	9.68	9.54	9.37	9.05	7.87	7.02	6.31	5.72	5.78	5.82	5.82	5.54	5.31	5.10	+0.813	-6.404

3.2.7. Potential adsorptive elimination of BF and MB dye from various water specimens

The validity of practical application of BCCW-NB nanobiosorbent in real adsorptive elimination of BF and MB dyes from various water specimens was also investigated and the results are collected in Table 6. It is evident and confirmed that the percentage removal values (R%) upon using 15 mg/L of MB dye were 98.58%, 91.07% and 98.55% from drinking water, sea water and industrial water, separately and 93.45%, 90.13% and 97.89% for BF dye from the same previous water specimens. Comparable results were also obtained by using the other two concentrations as listed in Table 6. Therefore, the data in this manuscript work emphasize the validity of BCCW-NB nanobiosorbent for water remediation of dyes pollutants.

4. Conclusion

A sustainable, ecofriendly, and low-cost nanobiosorbent was prepared by thermal conversion and pyrolysis of collected waste bare corn cobs. The produced nanobiochar (BCCW-NB) was characterized by different techniques providing uniform nanoparticles with average size ~ 25 nm according to the TEM analysis. The FT-IR analysis confirmed several functional groups as phenolic, C-O and O-H groups. The BET surface area, total pore volume and pore diameter of BCCW-NB nanobiochar at 77.4 K were identified as 9.077 m^2g^{-1}, 2.113x10^{-2} cm^3g^{-1} and 9.312 nm, respectively. The XRD pattern of BCCW-NB nanobiosorbent exhibited amorphous structure with a broad hump in the rang of 2θ = 15-30° due to the aromatic carbon skeleton. The impact of several factors on the batch elimination of BF and MB dyes from aqueous solution by BCCW-NB was investigated and optimized using three different concentrations of each dye (5, 10 and 15 mg/L). The optimum pH 5 and 30 mg BCCW-NB were characterized to afford the maximum removal of BF and MB dyes, while the adsorption conditions of BF and MB dyes were found to reach to the equilibrium at almost 10 min for both pollutants. The comparison of adsorption isotherm R^2 values revealed that Freundlich isotherm provided the best fitting for removal of BF and MB dyes onto BCCW-NB nanobiochar than the other evaluated models. Moreover, the computed kinetic R^2 values (0.999) by the *pseudo*-second-order model proved the adsorption of both dyes to the nanobiosorbent more than other kinetic models. Finally, the potential adsorptive elimination of BF and MB dyes from various water specimens confirmed excellent trends with R% = 98.58%, 91.07% and 98.55% for MB removal and 93.45%, 90.13% and 97.89% for BF dye from drinking water, sea water and industrial water. Therefore, the collected data in this work emphasized the validity for using BCCW-NB nanobiochar in water remediation of dye pollutants.

Table 6. Adsorptive removal of MB and BF dyes (initial concentrations: 5, 10 and 15 mg L^{-1}, from real water samples (mass =15 mg BCCW-NB nanobiosorbent, shaking time=10 min., pH=5 for both dyes, 20 mL dye solution)

Water sample	Removal (%) of MB dye			Removal (%) of BF dye		
	5 mg/L	10 mg/L	15 mg/L	5 mg/L	10 mg/L	15 mg/L
Tap water	97.69	98.20	98.59	92.01	93.40	93.45
Seawater	99.44	95.88	91.07	88.53	89.53	90.13
Wastewater	98.35	98.51	98.55	96.34	97.32	97.89

References

[1] Ramos, A.; Monteiro, E.; Rouboa, A.l. Biomass pre-treatment techniques for the production of biofuels using thermal conversion methods – A review, Energy Conver. Manag 2022, 270, 116271.

[2] Fu, X.; Zheng, Z.; Sha, Z.; Cao, H.; Yuan, Q.; Yu , H.; Li, Q. Biorefining waste into nanobiotechnologies can revolutionize sustainable agriculture, Trends in Biotechnol. 2022, 40, 1503-1518.

[3] Duque-Acevedo, M.; Belmonte-Ureña, L. J.; Cortés-García, F. J.; Camacho-Ferre, F. Agricultural waste: Review of the evolution, approaches and perspectives on alternative uses, Global Ecol. Conser. 2020, 22, e00902.

[4] Choi, J. Y.; Nam, J.; Yun, B. Y.; Kim, Y. U.; Kim, S. Utilization of corn cob, an essential agricultural residue difficult to disposal: Composite board manufactured improved thermal performance using microencapsulated PCM, Ind. Crops Prod. 2022, 183, 114931.

[5] Tsai, W.T.; Chang, C.Y.; Wang, S.Y.; Chien, C.F.; Chang, S.F.; Sun, H.F. Cleaner production of carbon

adsorbents by utilizing agricultural waste corn cob. Resour. Conserv. Recycl. 2001, 32 (2001) 43–53.

[6] Czajkowski, Ł.; Wojcieszak, D.; Olek, W.; Przybył, J. Thermal properties of fractions of corn stover. Constr. Build. Mater. **2019**, 210, 709–712.

[7] Tripathi, M.; Sharma, M.; Bala, S.; Connell, J.; Newbold, J. R.; Rees, R.M.; Aminabhavi, T. M.; Thakur, V. K.; Gupta, V. K. Conversion technologies for valorization of hemp lignocellulosic biomass for potential biorefinery applications, Sep. Purif. Technol. 2023, 320, 124018.

[8] Li, P.; Niu, B.; Pan, H.; Zhang, Y.; Long, D. Production of hydrocarbon-rich bio-oil from catalytic pyrolysis of waste cooking oil over nickel monoxide loaded corn cob-derived activated carbon, J. Clean. Prod. 2023, 384, 135653.

[9] Manmeen, A.; Kongjan, P.; Palamanit, A.; Jariyaboon, R. The biochar, and pyrolysis liquid characteristics, of three indigenous durian peel; Monthong, Puangmanee, and Bacho, Biomass and Bioenergy 2023, 174, 106816.

[10] Lu, Y.; Gu, K.; Shen, Z.; Tang, C.; Shi, B.; Zhou, Q. Biochar implications for the engineering properties of soils: A review, Sci. Total Environ. 2023, 888, 164185.

[11] T. He, M. Zhang, B. Jin, Co-pyrolysis of sewage sludge as additive with phytoremediation residue on the fate of heavy metals and the carbon sequestration potential of derived biochar, Chemosphere 2023, 314, 137646.

[12] Mahmoud, M.E.; Abou-Ali, S.A.A.; Elweshahy, S.M.T. Efficient and ultrafast removal of Cd (II) and Sm (III) from water by leaves of Cynara scolymus derived biochar. Mater. Res. Bull. 2021, 141, 111334.

[13] Mahmoud, M.E.; El-Bahy, S.M.; Elweshahy, S.M.T. Decorated Mn-ferrite nanoparticle@ Zn–Al layere double hydroxide@ Cellulose@ activated biochar nanocomposite for efficient remediation of methylene blue and mercury (II), Bioresource Technol. 2021, 342, 126029.

[14] Mahmoud, M.E.; El-Ghanam, A.M.; Saad, S.R. Sequential removal of chromium (VI) and prednisolone by nanobiochar-enriched-diamine derivative, Biomass Conv. Bioref. 2022, https://doi.org/10.1007/s13399-022-02888-1.

[15] Zhang, H.; Yao-Jen, T.; Duan, Y.; Liu, J.; Meng, L. Production of biochar from waste sludge/leaf for fast and efficient removal of diclofenac, J. Mol. Liq. 2020, 299, 112193.

[16] Liang, H.; Zhu, C.; Ji, S.; Kannan, P.; Chen, F. Magnetic Fe_2O_3/biochar composite prepared in a molten salt medium for antibiotic removal in water, Biochar 2022, 4, Article number: 3.

[17] Mahmoud, M.E.; Abdelfattah, A.M.; Tharwat, R.M.; Nabil, G.M. Adsorption of negatively charged food tartrazine and sunset yellow dyes onto positively charged triethylenetetramine biochar: Optimization, kinetics and thermodynamic study, J. Mol. Liq. 2020, 318, 114297.

[18] Zheng, Y.; Yang, Y.; Zhang, Y.; Zou, W.; Luo, Y.; Dong, L.; Gao, B. Facile one-step synthesis of graphitic carbon nitride-modified biochar for the removal of reactive red 120 through adsorption and photocatalytic degradation, Biochar 2019, 1, 89–96.

[19] Thillainayagam, B.P.; Nagalingam, R.; Saravanan P. Batch and column studies on removal of methylene blue dye by microalgae biochar. Biomass Conv Bioref. 2022, https:// doi. org/ 10. 1007/s13399- 022- 03038-3.

[20] Mahmoud, S.E.M.E.; Ursueguia, D.; Mahmoud, M.E.; Abdel-Fattah, T.M.; Díaz, E. Functional surface homogenization of nanobiochar with cation exchanger for improved removal performance of methylene blue and lead pollutants, Biomass. Conv. Bioref. 2023, https://doi.org/10.1007/s13399-023-04098-9.

[21] M.E.; Mahmoud, S.M.; Elsayed, Mahmoud, S.E.M.E.; Nabil, G.M.; Abdel Salam, M. Recent progress of metal organic frameworks-derived composites in adsorptive removal of pharmaceuticals, Polyhedron 2022, 226 (2022) 116082.

[22] Liang, L.; Xi, F.; Tan, W.; Meng, X.; B.; Hu, Wang, X. Review of organic and inorganic pollutants removal by biochar and biochar-based composites. Biochar 2022, 3, 255–281.

[23] J. Mittal, Recent progress in the synthesis of Layered Double Hydroxides and their application for the adsorptive removal of dyes: A review, J. Environ. Manag. 2021, 295 (2021) 113017.

[24] M.E.; Mahmoud, M.S.; Abdelwahab, Ibrahim, G.A.A. Surface functionalization of magnetic graphene oxide@ bentonite with α-amylase enzyme as a novel bionanosorbent for effective removal of Rhodamine B and Auramine O dyes, Mater. Chem. Phys. 2023, 301, 127638.

[25] Nazir, M.A.; Khan, N.A.; Cheng, C.; Shah, S.S.A.; Najam, T.; Arshad, M.; Sharif, A.; Akhtar, S.; Rehman, A. Applied clay science surface induced growth of ZIF-67 at Colayered double hydroxide: removal of methylene blue and methyl orange from water, Appl. Clay Sci. 2020, 190, 105564.

[26] Guo, X.; Yin, P.; Yang, H. Superb adsorption of organic dyes from aqueous solution on hierarchically porous composites constructed by ZnAl-LDH/Al (OH)3 nanosheets, Microporous Mesoporous Mater. 2018, 259, 123–133.

[27] Taheri, M.; Fallah, N.; Nasernejad, B. Which treatment procedure among electrocoagulation, biological, adsorption, and bio-adsorption processes performs best in azo dyes removal? Water Resour. Ind. 2022, 28, 100191.

[28] Xin, Y.; Zhou, L.; Ma, K.; Lee, J.; Qazi, H.I.; Li, A.; Bao, H.; Zhou, Y. Removal of bromoamine acid in dye wastewater by gas-liquid plasma: The role

of ozone and hydroxyl radical, J. Water Proc. Eng. 2020, 37, 101457.

[29] Peramune, D.; Manatunga, D.C.; Dassanayake, R.S.; Premalal, V.; Liyanage, R.N.; Gunathilake, C.; Abidi , N. Recent advances in biopolymer-based advanced oxidation processes for dye removal applications: A review, Environ. Res. Part 1, 2022, 215, 114242.

[30] Sarfo, D.K.; Kaur, A.; Marshall, D.L.; O'Mullane, A.P. Electrochemical degradation and mineralisation of organic dyes in aqueous nitrate solutions, Chemosphere 2023, 316, 137821.

[31] Rajesh, G.; Kumar, P.S.; Akilandeswari, S.; Rangasamy, G.; Lohita, S.; Shankar, V. ; Ramya, U.; Nirmala, M.; Thirumalai, K. Strategies for ameliorating the photodegradation efficiency of Mn-doped CdAl2O4 nanoparticles for the toxic dyes under visible light illumination, Chemosphere 2023, 321, 138069.

[32] Praveen, S.; Jegan, J.; Pushpa, T.B.; Gokulan, R.; Bulgariu, L. Biochar for removal of dyes in contaminated water: an overview Biochar 2022, 4, Article number: 10.

[33] Dwivedi, S.; Dey, S. Review on biochar as an adsorbent material for removal of dyes from waterbodies, Int. J. Environ. Sci. Technol. 2022, https://doi.org/10.1007/s13762-022-04364-9

[34] Sassi, W.; Ghanmi, I.; Oulego, P.; Collado, S.; Ammar, S.; Díaz, M. Pomegranate peel-derived biochar as ecofriendly adsorbent of aniline-based dyes removal from wastewater, Clean Techn. Environ. Policy 2023, https://doi.org/10.1007/s10098-023-02522-2.

[35] Oraon, A.; Prajapati, A.K.; Ram, M.; Saxena, V.K.; Dutta, S.; Gupta, A.K. Synthesis, characterization, and application of microporous biochar prepared from Pterospermum acerifolium plant fruit shell waste for methylene blue dye adsorption: the role of surface modification by SDS surfactant, Biomass Conv. Bioref. 2022, https://doi.org/10.1007/s13399-022-02320-8.

[36] Yılmaz, M.; Eldeeb, T. M.; Hassaan, M. A.; El-Nemr, M.A.; Ragab, S.; El Nemr, A. The Use of Mandarin-Biochar-O3-TETA (MBT) Produced from Mandarin Peels as a Natural Adsorbent for the Removal of Acid Red 35 (AR35) Dye from Water. Environ. Process. 2022, 9, https://doi.org/10.1007/s40710-022-00592-w.

[37] Viswanathan, S.P.; Njazhakunnathu, G.V.; Neelamury, S.P.; Padmakumar, B.; Ambatt, T.P. The efficiency of aquatic weed–derived biochar in enhanced removal of cationic dyes from aqueous medium, Biomass Conv. Bioref. 2022, https://doi.org/10.1007/s13399-022-03546-2.

[38] Li, L.; Zhang, H.; Liu, Z.; Su, Y.; Du, C. Recent Advances and Prospects of Biochar-based Adsorbents for Malachite Green Removal: A Comprehensive Review, Environ. Sci. Pollut. Res. 2023, 6, 579–608.

[39] Vishnu, D.; Dhandapani, B.; Panchamoorthy, G.; K.; Vo, D.N.; Ramakrishnan, S.R. Comparison of surface-engineered superparamagnetic nanosorbents with low-cost adsorbents of cellulose, zeolites and biochar for the removal of organic and inorganic pollutants: a review, Environm. Chem. Lett. 2021, 19, 181–3208.

[40] Abd-Elhamid, A.I.; Emran, M.; El-Sadek M.; H.; El-Shanshory, A.A.; Soliman, H.M.A.; Akl; M.A.; Rashad, M. Enhanced removal of cationic dye by eco-friendly activated biochar derived from rice straw, Appl. Water Sci. 2020, 10, Article number: 45.

[41] Mahmoud, M.E.; Osman, M.M.; Yakout, A.A.; Abdelfattah, A.M. Green nanosilica@ folic Acid (VB9) nanocomposite for engineered adsorptive water remediation of bivalent lead, cadmium and copper, Powder Technol. 2019, 344, 719-729.

[42] Liao, G.; He, W.; He, Y. Investigation of Microstructure and Photocatalytic Performance of a Modified Zeolite Supported Nanocrystal TiO_2 Composite, Catalysts. 2019, 9, 502.

[43] Bunaciu, A.A.; Udriştioiu, E.G.; Aboul-Enein, H.Y. X-Ray Diffraction: Instrumentation and Applications. Crit. Rev. Anal. Chem. 2015, 45, 289-299.

[44] Kamble, S.B.; Shindea, S.H.; Rode, C.V. Highly efficient triphenyl(3-sulfopropyl)phosphonium functionalized phosphotungstic acid on silica as a solid acid catalyst for selective mono-allylation of acetals, Catal.Sci.Technol. 2015, 5, 4039-4047.

[45] Mahmoud, M.E.; El-Said, G.F.; Rashedy, I.R.; Abdelfattah, A.M.; Assembly and implementation of an eco-friendly marine nanosediment for adsorptive removal of heptavalent manganese: Adsorption isotherm, thermodynamic and kinetics studies, Powder Technol. 2019, 359, 247-260.

[46] Huang, W.; Chen, J.; Zhang, J. Adsorption characteristics of methylene blue by biochar prepared using sheep, rabbit and pig manure, Environ. Sci. Pollut. Res., 2018, 25, 29256-29266.

[47] Lonappan, L.; Rouissi, T.; Das, R.K.; Brar, S.K.; Ramirez, A.A.;Verma, M.; Surampalli, R.Y.; Valero, J.R. Adsorption of methylene blue on biochar microparticles derived from different waste materials, J. Waste Manag. 2016, 49, 537-544.

[48] Mahmoud, M.E.; Nabil, G.M.; Khalifa, M.A.; El-Mallah, N.M.; Hassouba, H.M. Effective removal of crystal violet and methylene blue dyes from water by surface functionalized zirconium silicate nanocomposite, J. Environ. Chem. Eng, 2019, 7, 103009.

[49] Arora, C.; Soni, S.;Sahu, S.; Mittal, J.; Kumar, P.; Bajpai, P. Iron based metal organic framework for efficient removal of methylene blue dye from industrial waste, J. Mol. Liq. 2019, 284, 343-352.

[50] Doğan, M.; Alkan, M.; Demirbas, O.; Özdemir, Y.; Özmetin, C. Adsorption kinetics ofmaxilon blue GRL

onto sepiolite from aqueous solutions, Chem. Eng. J. 2019, 124, 89–101.

[51] Kemik, Ö.F.; Ngwabebhoh, F.A.; Yildiz, U. A response surface modelling study for sorption of Cu^{2+}, Ni^{2+}, Zn^{2+} and Cd^{2+} using chemically modified poly (vinylpyrrolidone) and poly (vinylpyrrolidone-co-methylacrylate) hydrogels, Adsor. Sci. Technol. 2017, 35, 263-283.

[52] Sharma, G.; Kumar, A.; Devi, K.; Sharma, S.; Naushad, M.; Ghfar, A.A.; Ahamad, T.; Stadler, F.J. Guar gum-crosslinked-Soya lecithin nanohydrogel sheets as effective adsorbent for the removal of thiophanate methyl fungicide, Int. J. Biol. Macromol. 2018, 114, 295-305.

[53] Ho, Y.-S.; McKay, G. Pseudo-second order model for sorption processes, Process Biochem. 1999, 34, 451-465.

[54] Weber W.J.; Morris, J.C. Kinetics of adsorption on carbon from solution, J. Sanit. Eng. Divis. 1963, 89, 31-60.

[55] Chien, S.; Clayton, W. Application of Elovich equation to the kinetics of phosphate release and sorption in soils, Soil. Sci. Soc. Am. J. 1980, 44, 265-268.

[56] Vadivelan, V.; Kumar, K.V. Equilibrium, kinetics, mechanism, and process design for the sorption of methylene blue onto rice husk, J. Colloid Interf. Sci. 2005, 286, 90-100.

[57] Mahmoud, M.E.; Nabil, G.M.; El-Mallah, N.M.; Karar, S.B. Improved removal and decolorization of CI anionic reactive yellow 145 A dye from water in a wide pH range via active carbon adsorbent-loaded-cationic surfactant, Desalination Water Treat. 2015, 55, 227-240.

[58] Langmuir, I. The adsorption of gases on plane surfaces of glass, mica and platinum, J. Am. Chem. Soc. 1918, 40, 1361-1403.

[59] Greluk, M.; Hubicki, Z. Kinetics, isotherm and thermodynamic studies of Reactive Black 5 removal by acid acrylic resins. Chem. Eng. J. 2010, 162, 919-926.

[60] Freundlich, H. Über die adsorption in lösungen, Zeitschrift für Physikalische Chem. 1907, 57, 385-470.

[61] Temkin, M. Kinetics of ammonia synthesis on promoted iron catalysts, Acta Physiochim. URSS, 1940, 12, 327-356.

[62] Günay, A.; Arslankaya, E.; Tosun, I. Lead removal from aqueous solution by natural and pretreated clinoptilolite: adsorption equilibrium and kinetics, J. Hazard. Mater. 2007, 146, 362-371.

[63] Kalavathy, M.H.; Miranda, L.R. Comparison of copper adsorption from aqueous solution using modified and unmodified Hevea brasiliensis saw dust, Desalination 2010, 255, 165-174.

[64] Wu, Y.; Zhang, S.; Guo, X.; Huang, H. Adsorption of chromium (III) on lignin, Bioresour. Technol. 2008, 99, 7709-7715.

[65] Alshabanat, M.; Alsenani, G.; Almufarij, R. Removal of crystal violet dye from aqueous solutions onto date palm fiber by adsorption technique, Int. J. Chem. 2013, (2013). https://doi.org/10.1155/2013/210239.

[66] Chen, F.-x.; Zhou, C.-r.; Li, G.-p.; Peng, F.-f. Thermodynamics and kinetics of glyphosate adsorption on resin D301, Arab. J. Chem. 2016, 9, S1665-S1669.

[67] Wang, Y.; Liu, W.; Zhang, L.; Hou, Q. Characterization and comparison of lignin derived from corncob residues to better understand its potential applications , Int. J. Biol. Macromol. 2019, 134, 20–27.